# Supporting Information

# $TaO_x$-based self-rectifying memristor for highly compact thermal in-sensor computing

Lijuan Cao[a], Yunhao Luo[a], Jiaping Yao[a], Xiang Ge[a], Maoyuan Luo[a], Jiaqi Li[a], Xiaomin Cheng[a *], Rui Yang[a], Xiangshui Miao[a]

[a]School of Integrated Circuits, Hubei Key Laboratory for Advanced Memories, Wuhan National Laboratory for Optoelectronics, Huazhong University of Science and Technology, Wuhan 430074, China

**E-mail: xmcheng@hust.edu.cn**

## 1. The actual optical microscope and cross-sectional SEM images

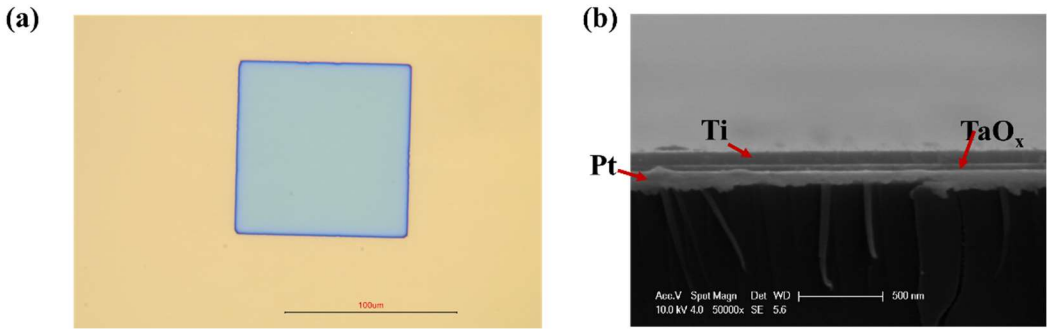


**Figure S1.** The actual optical microscope and cross-sectional SEM images Ti/$TaO_x$/Pt device. (a)The actual optical microscope image. (b) The cross-sectional SEM image.

## 2. I-V curves under different applied voltage ranges

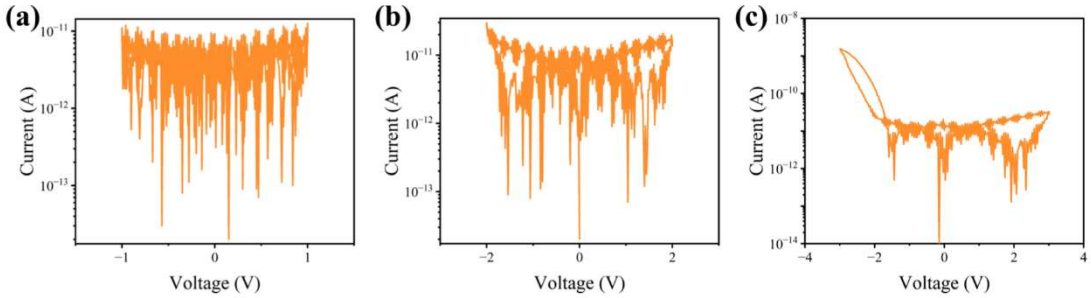


**Figure S2.** I-V curves under different applied voltage ranges of Ti/$TaO_x$/Pt device. (a) Voltage sweep from -1V to 1V. (b) Voltage sweep from -2V to 2V. (c) Voltage sweep from -3V to 3V.

## 3. Device to device uniformity

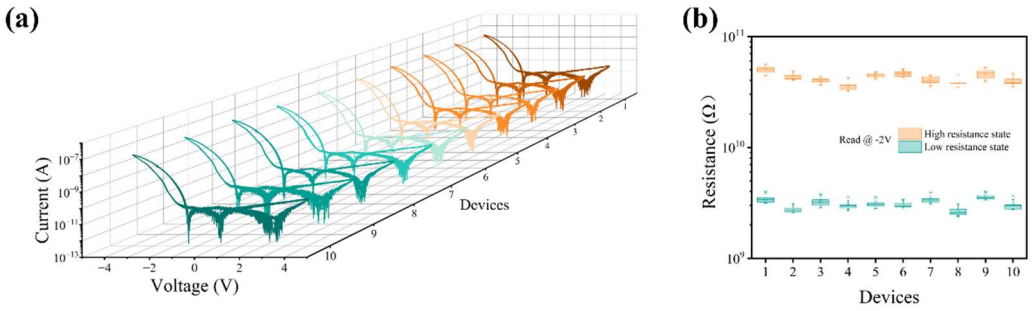


**Figure S3.** The device-to-device uniformity of Ti/$TaO_x$/Pt device. (a) I–V curves of 10 independent devices (each device tested under 10 cycles). (b) High resistance state and low resistance state distributions for the 10 devices of (a).

## 4. I-V curves under different temperatures

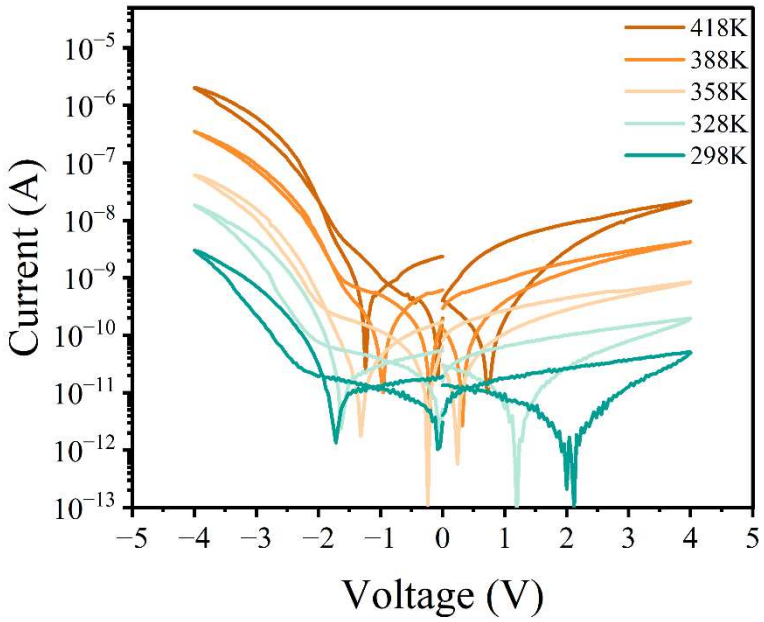


**Figure S4.** I-V curves under different temperatures (298K-418K, interval 30K)

## 5. Mechanism analysis

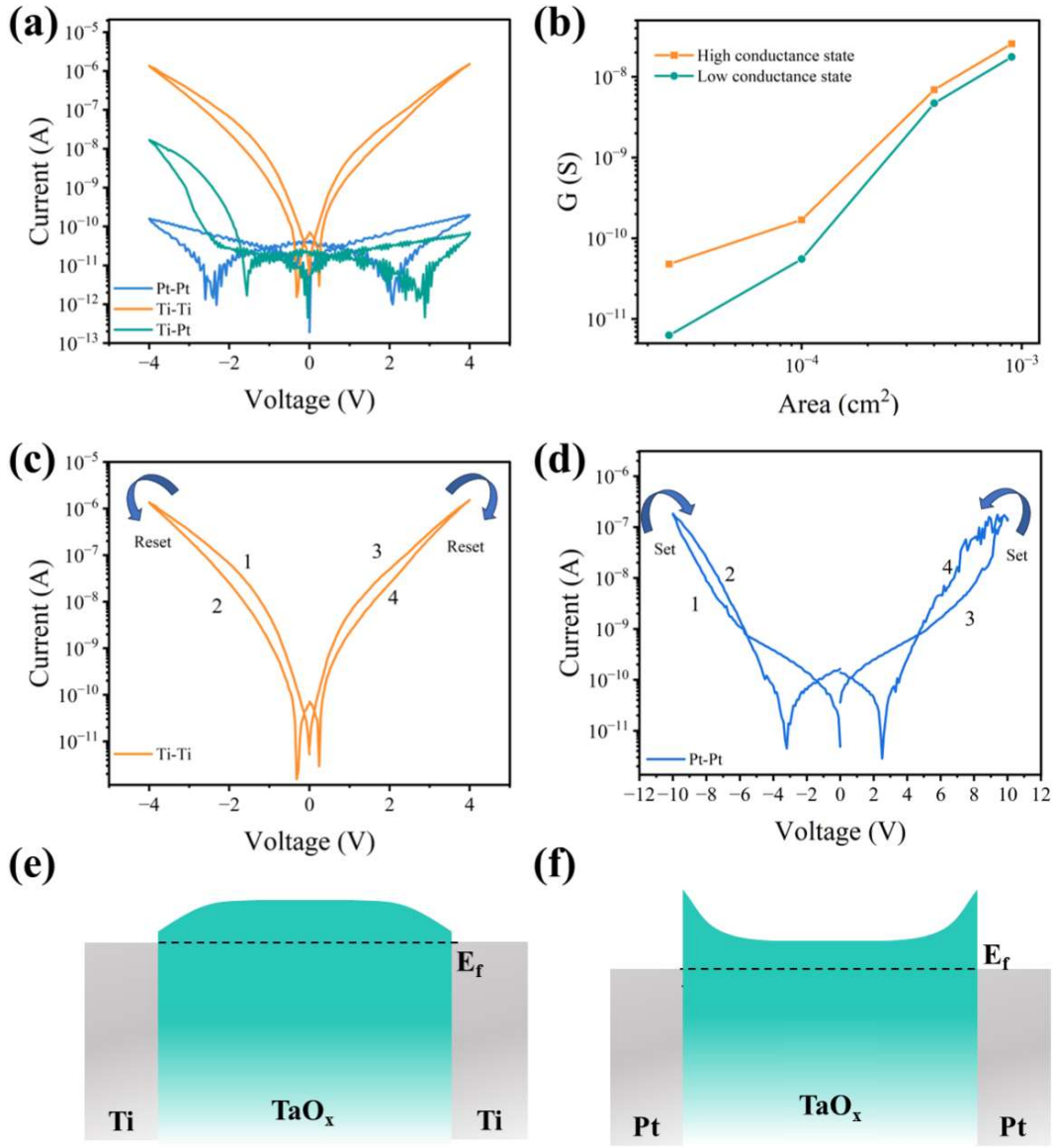


**Figure S5.** The RS mechanism analysis of Ti/$TaO_x$/Pt device. (a) The I-V curves of the Ti/$TaO_x$/Pt (TOP), Ti/$TaO_x$/Ti (TOT), and Pt/$TaO_x$/Pt (POP) devices. Only the TOP device shows self-rectification characteristics, meaning that a work function difference between the two electrodes is necessary for achieving self-rectification. (b) The relationship between the area and the Ti/$TaO_x$/Pt device's conductance states. The high conductance and low conductance states are area-dependent, indicating that its RS behavior is not filament-type. (c) The I-V curve of TOT device. The TOT device is in reset process no matter what direction of voltage is applied. (d) The I-V curve of POP device. The POP device is in set process no matter what direction of voltage is applied.

(e) The band structure of the TOT device. Since the work function of the Ti is lower than that of $TaO_x$, electrons easily flow over the barrier from metal into the $TaO_x$ film and then are captured by the trap levels. Therefore, the device is initially in a low resistance state. When an external electric field is applied, electrons easily flow from $TaO_x$ layer to Ti electrode which make the device reset. (f) The band structure of POP device. Since the work function of Pt is higher than that of $TaO_x$, electrons easily flow over the barrier from $TaO_x$ layer into Pt electrode. Therefore, the device is initially in a high resistance state. When an external electric field is applied, electrons are easily flow from Pt electrode to $TaO_x$ layer which make the POP device set. In summary, the carrier trapping-detrapping mechanism can well explain the RS processes of TOT and POP devices, and further confirm that the RS mechanism of TOP device is based on the carrier trapping-detrapping mechanism rather than filament mechanism.

## 6. The I-V fitting result in low voltage region

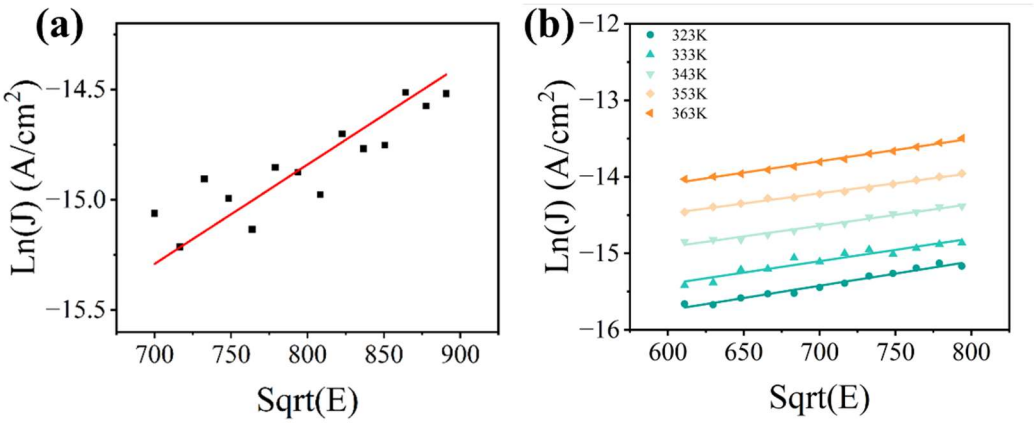


**Figure S6.** I–V curve fitting result of Ti/$TaO_x$/Pt device in low voltage region. (a) I–V curve fitting result in low voltage region at 300K. (b) I–V curve fitting result in low voltage region at different temperatures (323K-363K). The dynamic dielectric constant of tantalum oxide can be calculated within the range of 7.34~13.17. The Schottky barrier calculated by fitting is 0.25-0.3eV, which is close to the UPS test result.

## 7. The detailed derivation of equation (2) in the article

The $\sigma_0$ is given by[1]

$$\sigma_0 = nq\mu \tag{S1}$$

where $n$ is the free carrier density, $q$ is the elementary charge and $\mu$ is the carrier mobility. The free carrier density $n$ and trapped carrier density $n_t$ are respectively given by[1]

$$n = N_c \exp\left(-\frac{E_C - E_F}{kT}\right) \tag{S2}$$

$$n_t = N_t \exp\left(-\frac{E_t - E_F}{kT}\right) \tag{S3}$$

where $N_c$ is the effective density of states in the conduction band, $N_t$ is the density of traps, $E_C$ and $E_t$ are the conduction-band energy level and the trap energy level, respectively, and $E_F$ is the Fermi energy level. From equations (S1), (S2) and (S3), we can obtain

$$\sigma_0 = q\mu N_c \frac{n_t}{N_t} \exp\left(-\frac{E_C - E_t}{kT}\right) \tag{S4}$$

## 8. The optical dielectric constant of $TaO_x$ film.

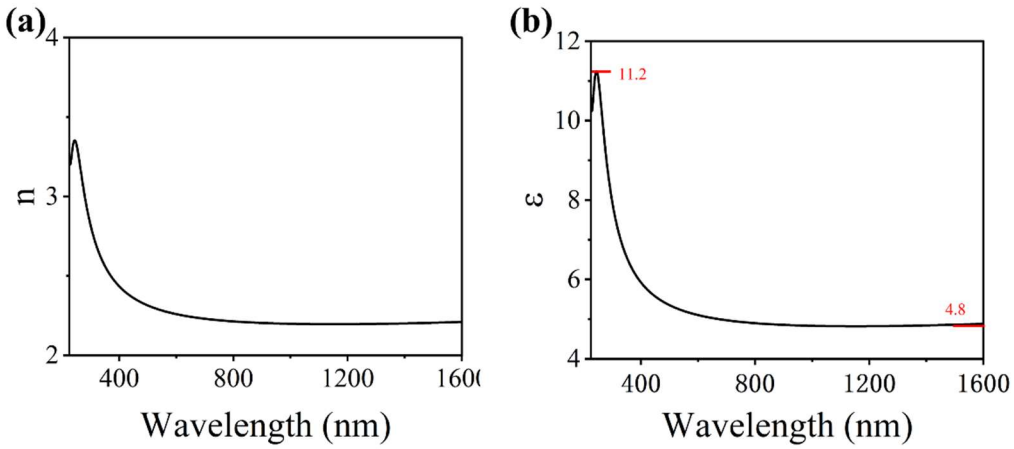


Figure S7. The optical refractive index and optical dielectric constant of $TaO_x$ film (a) The optical refractive index of $TaO_x$ measured by the ellipsometer. (b) The optical dielectric constant of $TaO_x$ film calculated using the optical refractive index.

## 9. The characteristics of nonlinear integration of input information

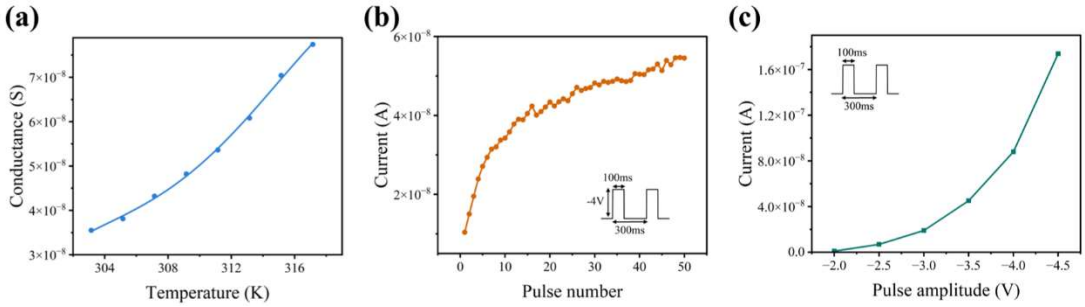


**Figure S8.** Nonlinear input information integration characteristics of Ti/$TaO_x$/Pt device. (a) The superlinear relationship between temperature and the conductance of Ti/$TaO_x$/Pt device. (b) Current responses sublinearly to input pulse number. (c) Current responses superlinearly to input pulse amplitude.

## 10. The I-V curves of each device in the 3×3 array, the temperature input images and the current results of each device

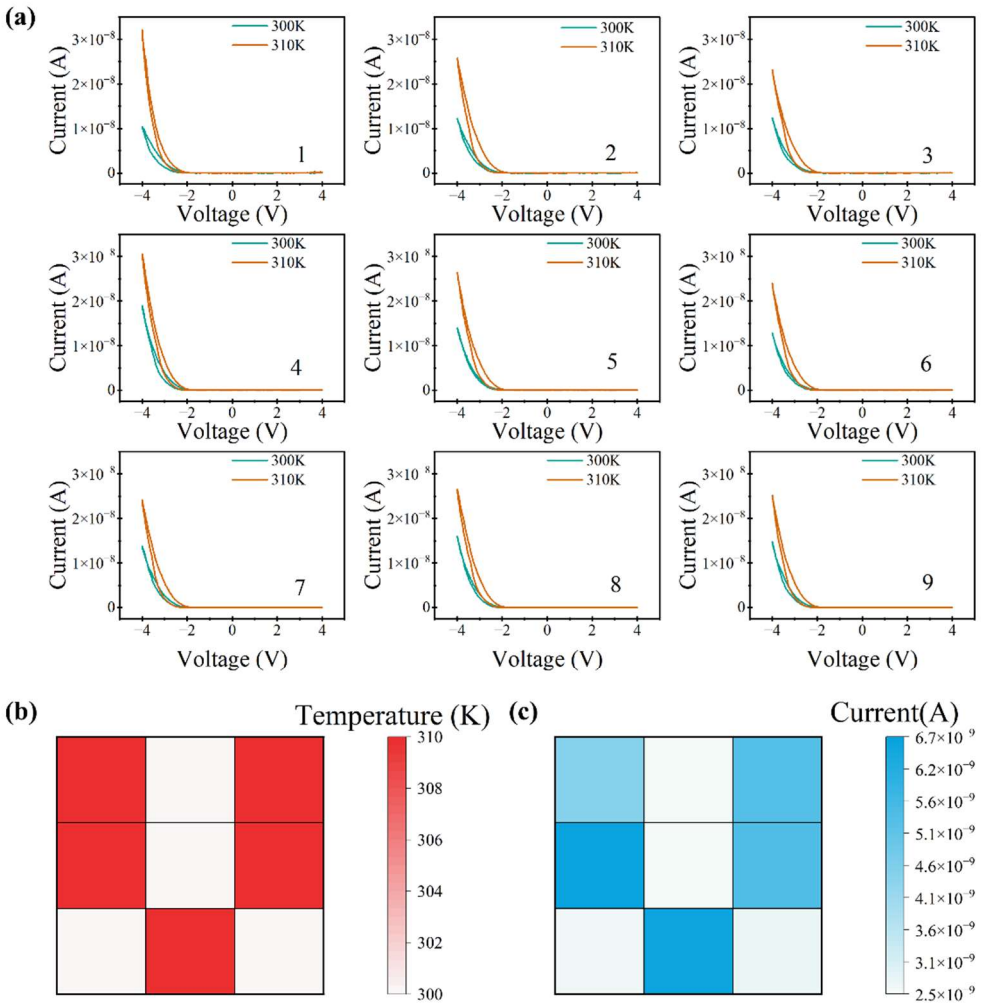


**Figure S9**. (a) The I-V curves of each device in the 3×3 array. (b) Input temperature image (b) The current distribution image after the array input temperature image.

## 11. The compact model of Ti/$TaO_x$/Pt device

In order to build the circuit simulation of the leaky-integrated-and-fire (LIF) neurons, we constructed the compact model of Ti/$TaO_x$/Pt device.

The current density $J$ of the device is given by

$$J = E\sigma \tag{S5}$$

where $E$ is extra electric field, $\sigma$ is the conductivity as a function of electrical field. From equations (1), (2), (S5), the current is

$$I = Sq\mu EN_c \exp\left(-\frac{\emptyset_t - (q^3E/\pi\epsilon_0\epsilon)^{1/2}}{kT}\right)\cdot\theta \tag{S6}$$

where $S$ is the device area, $q$ is the elementary charge, $\mu$ is the carrier mobility, $E$ is the electrical field, $N_c$ is the effective density of states in the conduction band, $\epsilon_0$ is the permittivity of free space, $\epsilon$ is the dynamic dielectric constant, $k$ is the Boltzmann constant, $T$ is the temperature, $\emptyset_t$ is the trap energy level, and $\theta$ is the trap-filled probability. The current response of the device is proportional to the trap-filled probability, according to equation (S6).

Among them, the effective density of states in the conduction band can be expressed as

$$N_C = 2\left(\frac{2\pi m_n^* kT}{h^2}\right)^{\frac{3}{2}} \tag{S7}$$

where $m_n^*$ is the effective electron mass, $h$ is the Planck constant.

By converting equation (S6) and (S7), the $\theta$ is the trap-filled probability can be expressed as

$$\theta = \frac{I}{2Sq\mu E\left(\frac{2\pi m_n^* kT}{h^2}\right)^{\frac{3}{2}} exp\left(-\frac{\emptyset_t - (q^3E/\pi\epsilon_0\epsilon)^{1/2}}{kT}\right)} \tag{S8}$$

where the parameters except the current value are shown in Table **S1**.

Therefore, the key to constructing the compact model of Ti/$TaO_x$/Pt device is to find the relationship between $\theta$ and time. We assume that the traps in the $TaO_x$ film only have two states (the carrier-filled and unfilled states) [2]. **Figure S6**a shows the trap transition between the carrier-filled and unfilled states, where $K_1$ and $K_2$ are the

transition rates from unfilled state to filled state and from filled state to unfilled state, respectively. The trap-filled probability $\theta(t)$ can also be given by[2]

$$\frac{d\theta(t)}{dt} = K_1 \cdot \big(1 - \theta(t)\big) + K_2 \cdot \theta(t) \qquad (S9)$$

The equation (S9) can be solved by[2]

$$\theta(t) = \theta(\infty) + \big(\theta(0) - \theta(\infty)\big) \cdot e^{-\frac{t}{\tau}} \qquad (S10)$$

where

$$\theta(\infty) = \frac{K_1}{K_1 + K_2} \qquad (S11)$$

$$\tau = \frac{1}{K_1 + K_2} \qquad (S12)$$

At the same time, $K_1$ and $K_2$ are respectively given by[3]

$$K_1 = A_1 \cdot \exp(-V \cdot B_1 + C_1) + D_1 \qquad (S13)$$

$$K_2 = A_2 \cdot \exp(V \cdot B_2 + C_2) + D_2 \qquad (S14)$$

where $A_1$, $A_2$, $B_1$, $B_2$, $C_1$, $C_2$, $D_1$, $D_2$ can be fitted by the values of $K_1$ and $K_2$ at different voltages, $V$ is the applied voltage.

To fitted the values of $A_1, A_2, B_1, B_2, C_1, C_2, D_1, D_2$, we need to get the values of $K_1$ and $K_2$ at different voltages. The values of $K_1$ and $K_2$ at different voltages can be fitted with the values of $\theta(t)$ at different voltages by equation (S10). And the values of $\theta(t)$ at different voltages can be calculated by equation (S8), which are shown in **Figure S10**b.

In order to represent the change of $\theta(t)$ over time, the equation (S9) is converted into a sub-circuit[3], as shown in **Figure S10c**. Where, the change of $\theta(t)$ with time is represented by the voltage at point A. Subsequently, the current of the device $I$ can be obtained by formula (S6). **Table S1** summarizes the model parameters extracted by the above equations and methods. **Figure S10d** demonstrates the agreement between the compact model simulations results and the measurement results. The result shows that this compact model can be used in circuit simulation of the LIF neurons constructed by Ti/$TaO_x$/Pt device.

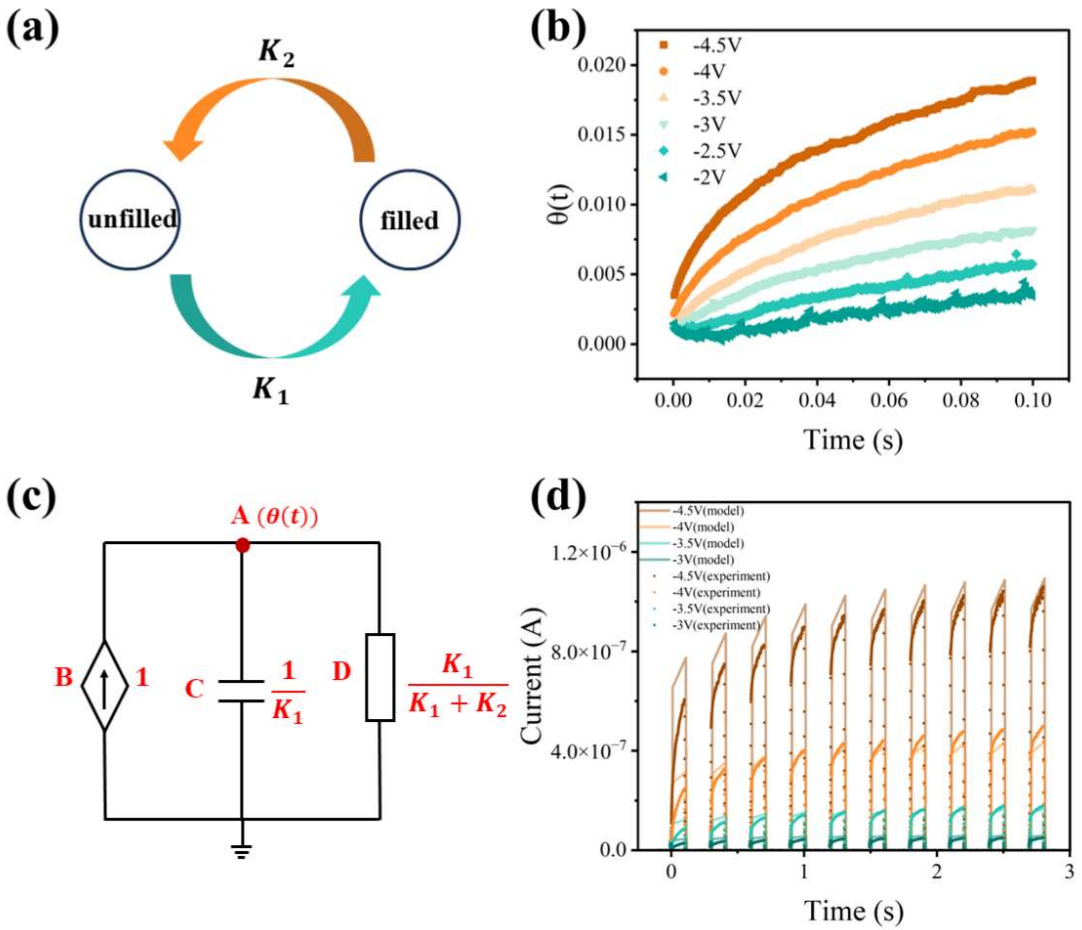


**Figure S10.** Ti/$TaO_x$/Pt device compact model and simulation results. (a) State transition process diagram for two-state (filled and unfilled) traps. $K_1$ and $K_2$ are the transition rates from unfilled state to filled state and from filled state to unfilled state, respectively. (b) The trap filling probability changes over time at different voltages. (c) Subcircuit diagram representing the electron filling level of the trap. Where, the value of $\theta(t)$ is represented by the voltage at point A; The B device is a current source with a value of 1; The C device is capacitor with a value of $1/K_1$; The D device is a resistor with a value of $K_1/(K_1+K_2)$. (d) Fitting of the simulation results of the device compact model with experimental results (input pluses: -4V 100ms) under different voltage amplitudes.

**Table S1 Parameters of the compact model**

| $\boldsymbol{\mu}$ [4] $(\boldsymbol{cm^2/V\cdot s})$ | $\boldsymbol{T}$ $(\boldsymbol{K})$ | $\boldsymbol{m_n^*}$ [5] $(m_0)$ | $\boldsymbol{q}$ $(\boldsymbol{C})$ | $\boldsymbol{k}$ $(\boldsymbol{eV/K})$ |
|---|---|---|---|---|
| 22.535 | 300 | 2.7 | 1.6e-19 | 8.617e-5 |
| $\boldsymbol{\emptyset_t}$ [6] $(\boldsymbol{eV})$ | $\boldsymbol{\epsilon}$ [7] | $h$ $(\boldsymbol{J\cdot s})$ | $\boldsymbol{\epsilon_0}$ $(\boldsymbol{F/cm})$ | $\boldsymbol{d}$ $(\boldsymbol{cm})$ |
| 0.8 | 10 | 6.63E-34 | 8.85e-14 | 4e-6 |
| $\boldsymbol{s}$ $(\boldsymbol{cm^2})$ | $\boldsymbol{A_1}$ | $\boldsymbol{A_2}$ | $\boldsymbol{B_1}$ | $\boldsymbol{B_2}$ |
| 1e-4 | 0.01125 | 0.90354 | 0.478255443 | 0.36161 |
| $\boldsymbol{C_1}$ | $\boldsymbol{C_2}$ | $\boldsymbol{D_1}$ | $\boldsymbol{D_2}$ | |
| $-1.09515$ | 0.94309 | 0.00458 | $-0.50373$ | |

## References


[1] S.M. Sze, K.K. Ng, Physics of Semiconductor Devices, 1st ed., Wiley, 2006. https://doi.org/10.1002/0470068329.

[2] T. Grasser, Stochastic charge trapping in oxides: From random telegraph noise to bias temperature instabilities, Microelectron. Reliab. 52 (2012) 39–70. https://doi.org/10.1016/j.microrel.2011.09.002.

[3] Y. Li, X. Huang, C. Liao, R. Wang, S. Zhang, L. Zhang, R. Huang, A dynamic current hysteresis model for IGZO-TFT, Solid-State Electron. 197 (2022) 108459. https://doi.org/10.1016/j.sse.2022.108459.

[4] Q. Zhao, M. Cui, T. Liu, Charge Carrier Transport Mechanism in Ta2O5, TaON, and Ta3N5 Studied by Applying Polaron Hopping and Bandlike Models, ChemPhysChem 23 (2022) e202100859. https://doi.org/10.1002/cphc.202100859.

[5] M.V. Ivanov, T.V. Perevalov, V.S. Aliev, V.A. Gritsenko, V.V. Kaichev, Electronic structure of δ-Ta2O5 with oxygen vacancy: ab initio calculations and comparison with experiment, J. Appl. Phys. 110 (2011) 024115. https://doi.org/10.1063/1.3606416.

[6] W.S. Lau, L.L. Leong, T. Han, N.P. Sandler, Detection of oxygen vacancy defect states in capacitors with ultrathin Ta2O5 films by zero-bias thermally stimulated current spectroscopy, Appl. Phys. Lett. 83 (2003) 2835–2837. https://doi.org/10.1063/1.1616990.

[7] J.S. Lee, S.J. Chang, J.F. Chen, S.C. Sun, C.H. Liu, U.H. Liaw, Effects of O2 thermal annealing on the properties of CVD Ta2O5 thin films, Mater. Chem. Phys. 77 (2003) 242–247. https://doi.org/10.1016/S0254-0584(01)00559-4.